

DiP: A Scalable, Energy-Efficient Systolic Array for Matrix Multiplication Acceleration

Ahmed J. Abdelmaksoud, Shady Agwa and Themis Prodromakis

Abstract—Transformers are gaining increasing attention across Natural Language Processing (NLP) application domains due to their outstanding accuracy. However, these data-intensive models add significant performance demands to the existing computing architectures. Systolic arrays are spatial architectures that have been adopted by commercial AI computing platforms (like Google TPUs), due to their energy-efficient approach of data-reusability. However, these spatial architectures face a penalty in throughput and energy efficiency due to the need for input and output synchronization using First-In-First-Out (FIFO) buffers.

This paper proposes a novel scalable systolic-array architecture featuring Diagonal-Input and Permutated weight-stationary (DiP) dataflow for the acceleration of matrix multiplication. The proposed architecture eliminates the synchronization FIFOs required by state-of-the-art weight stationary systolic arrays. Aside from the area, power, and energy savings achieved by eliminating these FIFOs, DiP architecture maximizes the computational resources (PEs) utilization. Thus, it outperforms the weight-stationary counterparts in terms of throughput by up to 50%. Analytical models are developed for both weight stationary and DiP architectures, including latency, throughput, time to full PEs utilization, and FIFOs overhead. Additionally, a comprehensive hardware design space exploration is demonstrated using commercial 22nm technology, highlighting the scalability advantages of DiP over the conventional approach across various dimensions where DiP offers improvement of energy efficiency per area up to 2.02x. Furthermore, DiP is evaluated using various transformer workloads from widely-used models, consistently outperforming TPU-like architectures, achieving energy improvements of up to 1.81x and latency improvements of up to 1.49x across a range of transformer workloads. At a 64x64 size with 4096 PEs, DiP achieves a peak performance of 8.2 TOPS with energy efficiency 9.55 TOPS/W.

Index Terms—Hardware Acceleration, Systolic Arrays, Spatial Architectures, Matrix Multiplication, Weight Stationary.

I. INTRODUCTION

ARTIFICIAL Intelligence (AI) is continuously dominating various application domains that are vital in our daily life [1]. Natural Language Processing (NLP) is one of the emerging AI applications that are gaining an increasing attention nowadays [2, 3]. Thanks to Transformers, NLP tasks have been revolutionized by providing highly effective and scalable models for language understanding and generation [4]. The

This work was supported by EPSRC FORTE Programme (Grant No. EP/R024642/2) and by the RAEng Chair in Emerging Technologies (Grant No. CiET1819/2/93)

Ahmed J. Abdelmaksoud, S. Agwa and T. Prodromakis are with the Centre for Electronics Frontiers, Institute for Integrated Micro and Nano Systems, School of Engineering, The University of Edinburgh, EH9 3BF, Edinburgh, United Kingdom (e-mails: a.j.abdelmaksoud@ed.ac.uk; shady.agwa@ed.ac.uk; t.prodromakis@ed.ac.uk).

exceptional capabilities of these new NLP models have led to a transformer-driven transformation across numerous application domains, including Machine Translation [5], Speech Recognition [6], Multimodal Applications [7], and Computer Vision [8].

However, transformers are data-intensive models that handle massive workloads in comparison to Deep Neural Networks (DNNs) and Convolutional Neural Networks (CNNs) [9]. Additionally, transformer models have been growing exponentially, evolving from the original vanilla transformer model with around 65 million parameters to models with hundreds of billions of parameters [10, 11]. A clear example of the new challenging level of scalability is GPT (Generative Pre-trained Transformer) model (the core of ChatGPT) that incorporates billions of parameters, primarily involving matrix multiplications [12].

Conventional Von-Neumann architectures are struggling to meet these increasing performance demands due to the memory/data-movement bottleneck. Systolic arrays, introduced in 1970s, are spatial architectures that aim at maximizing the data utilization to mitigate the memory/data-movement bottleneck; These architectures are receiving increased attention nowadays as a promising architecture for AI hardware acceleration [13]. Usually, the systolic array consists of a set of two-dimensional (2D) interconnected Processing Elements (PEs). The PE is composed of basic arithmetic, mainly multiplication and accumulation, along with register units. Systolic arrays are spatial architectures that enhance local data utilization by increasing the number of computation operations per each memory access. Accordingly, data flows among different PEs in a wave fashion, while the communication with the synchronization First-In-First-Out (FIFO)s occurs only at the boundary PEs. Moreover, the interconnection of the systolic array naturally realizes data reuse through the interchange of data via PEs, especially in matrix multiplications [14].

Although many systolic arrays are extensively used for hardware accelerators [15–21], different adopted dataflows require further synchronization interfacing hardware that limits not only the energy efficiency, but also the performance capabilities of these dataflows. Therefore, transformers with massive matrix multiplication workloads will have serious challenges to leverage the systolic array scalability for a next generation of AI hardware.

Tensor Processing Unit (TPU) is one of the well-known AI computing architectures that is introduced by Google to handle massive matrix multiplication workloads with higher performance and energy efficiency than CPUs and GPUs [22]. TPUs adopt weight stationary dataflow, which maximizes the

This work has been submitted to the IEEE for possible publication.

Copyright may be transferred without notice, after which this version may no longer be accessible.

data utilization of both weights and inputs. The first-generation TPU (TPU v1) is designed primarily for inference, featuring a 256x256 systolic array optimized for 8-bit integer (INT8) operations, achieving a peak throughput of 92 TOPS [23]. TPU v2 shifted to mixed-precision training with a smaller 128x128 systolic array per core optimized for FP16 and bfloat16 operations, boosting throughput to 180 TeraFLOPS [24]. TPU v3 and v4 maintained the same array size but v3 doubled the throughput to 420 TFLOPS per chip, aided by high memory bandwidth, while TPU v4 uses four cores of 128x128 architecture, achieving up to 1 PFLOPS [25]. In conventional WS systolic array, synchronization FIFOs are necessary to synchronize both inputs and outputs, adding significant overhead in terms of throughput, energy, latency, power, and area. Moreover, the computations propagate as a diagonal wavefront from the top-left corner to the bottom-right corner of the systolic array due to the WS dataflow. This significantly decreases the overall PEs utilization resulting in degraded performance and increased latency.

Meissa is one of systolic architectures that separates multipliers from the adders rather than combining them in a unified array [26]. It stands for multiplying matrices efficiently in a scalable systolic architecture. Like to the TPUs, it adopted the WS dataflow for the systolic array, but it eliminates the input synchronization FIFOs to reduce the overall latency. However, it has bulky adder trees per each column of the systolic array instead of having the partial summations accumulated through the PEs. These adder trees impose scalability limitations due to serious physical implementation challenges. The larger the adder trees the deeper pipelines they require to achieve higher frequency. This increases the overall latency, area, and energy consumption. The routing congestion is another expensive challenge, caused by delivering all products from all PEs in the same column to the adder tree. Consequently, Meissa is not scalable to large NxN dimensions, which is vital to large language models. Moreover, it still requires the output synchronization FIFOs which still add a considerable area/power/energy penalty.

In this paper, we present a novel Diagonal-Input Permuted (DiP) weight-stationary Systolic Array that overcomes the main challenges of the conventional WS systolic arrays. DiP is a scalable architecture of NxN PEs that maximizes the PEs utilization by featuring diagonal-input movement and permuted weight-stationary dataflow for the acceleration of matrix multiplication.

The main contributions of this work are highlighted as follows:

- We introduce DiP, a novel scalable spatial architecture that maximizes the PEs utilization and energy efficiency achieving improvement in throughput by up to 1.49x and energy efficiency per area by up to 2.017x.
- The proposed architecture eliminates the input/output synchronization FIFOs of the WS by implementing a new dataflow with diagonal-input movement and permuted weights.
- The analytical models for DiP and WS including throughput, latency, time to full PEs utilization (TFPU), and

registers overhead are extracted for different systolic array sizes.

- Hardware Design space exploration and implementation are presented for DiP and WS using commercial 22nm technology, offering energy efficiency per area improvement up to 2.02x with area and power consumption savings up to 8.12% and 19.95%, respectively.
- DiP is evaluated using various transformers workloads from widely-used models, outperforming TPU-like architectures, and achieving energy improvement up to 1.81x and latency improvement up to 1.49x across various transformer workloads.

This paper is organized as follows; Section II discusses the systolic arrays background. Section III presents DiP architecture. Section IV shows hardware design space exploration, evaluation, and results. Finally, section V concludes the work.

II. SYSTOLIC ARRAYS BACKGROUND

Systolic arrays usually adopt one of the dataflows to control the data movement across the PEs. Each dataflow retains one of the input/output/weight data to be stationary during computations for the maximum duration to exploit the data reuse [27, 28]. The following dataflows are the most common for the systolic array design:

- Weight Stationary (WS): weights are initially loaded to PEs and kept stationary during processing. The input matrix and partial summations are moved among PEs during processing.
- Input Stationary (IS): input matrix is initially loaded to the systolic array, while weight matrix and partial summations are moved among PEs during processing.
- Output Stationary (OS): input and weight matrices are moved across the PEs, while the partial summations are accumulated inside the PEs.
- Row Stationary (RS): This dataflow is proposed by Eyeriss [29]. It adopts spatial architecture that uses coarse-grained PEs with internal memories to store weights and inputs. Inputs are broadcasted diagonally across the PEs, while weight matrix broadcasted horizontally, and partial summations move vertically.

OS dataflow moves both input and weight matrices simultaneously, which effectively doubles the required memory bandwidth for the systolic array. With RS dataflow, data redundancy increases because copies of the data are loaded into different PEs. Additionally, the circulation of weights within each PE reduces energy efficiency. On the other hand, the WS dataflow is widely used in many architectures, such as the Google TPU, due to its scalability and flexibility in handling convolutions and matrix multiplication [23–25]. Additionally, it requires less memory bandwidth. Therefore, we will focus on improving it.

A. WS Dataflow

WS dataflow is widely used in many architectures where weights are initially loaded to the systolic array's PEs, while input matrix circulates among the PEs in a systolic fashion.

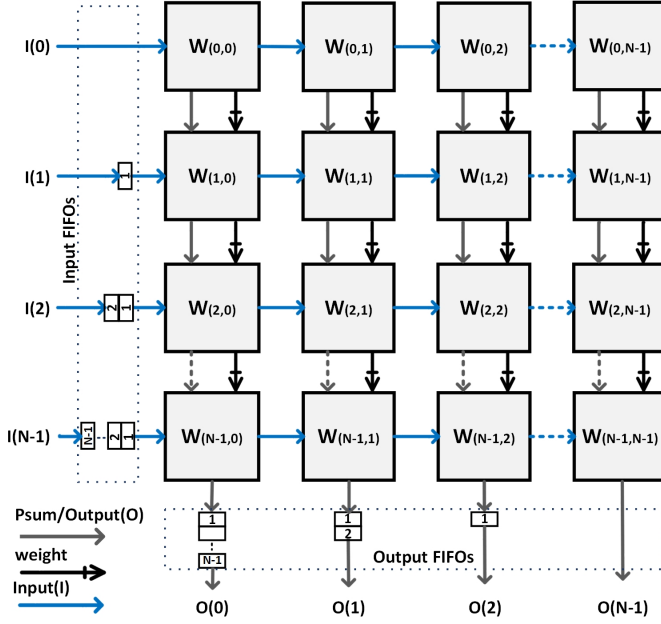


Fig. 1. Top-level schematic for $N \times N$ weight stationary systolic array. There are two FIFO groups for input/output synchronization. The weights (black crossed buses) are loaded vertically, and psums (grey buses) are accumulated vertically. Inputs (I) (blue buses) are shifted horizontally from the input FIFO group, and the output is shifted out to the output FIFO group.

This approach mitigates the memory bottleneck by reducing the number of memory accesses and increasing data reusability. However, the WS dataflow requires input and output FIFOs to synchronize the data for proper functionality. Figure 1 shows $N \times N$ weight stationary systolic array. There are two FIFO groups for input/output synchronization. The input FIFO group consists of series of FIFOs with incrementally increasing depth starting from one element in the second row up to $N - 1$ elements in the last row. The output FIFO group is structured similarly to the input FIFO group, but the FIFO depths decrease from $N - 1$ elements to one element moving from left to right across the systolic array columns. Weights are loaded vertically, and partial summations (psums) are accumulated vertically. Input matrix is shifted horizontally from the input FIFO group, and the output from the last PE row is shifted out to the output FIFO group. The use of FIFOs increases area, power, energy consumption, and latency for matrix multiplication. Consequently, FIFO-based systolic arrays suffer from lower energy efficiency, and reduced PE utilization, leading to higher latency and decreased throughput.

The analytical modeling of the WS systolic array is studied for latency, throughput, TFPU, and FIFOs overhead, providing insights into dataflow performance. For the WS latency analytical model, as shown in (1), WS requires $3N + S - 3$ cycles to complete the processing, where N represents the number of rows/columns per WS systolic array, and S is the number of pipeline stages per Multiply-Accumulate (MAC) unit, equals one for 1-stage pipelined MAC, and two for 2-stage pipelined MAC. The throughput, as indicated in (2), is calculated as the ratio of total operations to WS latency. Regarding register overhead, WS systolic array uses two FIFO

groups for input and output synchronization. Each group consists of $N - 1$ FIFOs, as shown in Fig. 1. Additionally, each FIFO group includes $N(N - 1)/2$ registers. Consequently, the total register overhead for a typical WS systolic array is calculated as shown in (3). TFPU is another metric introduced to calculate the required number of cycles to reach full utilization of PEs. This metric shows the overhead when the input matrix is initially loaded to PEs. TFPU is calculated, as shown in (4), where it takes $2N - 1$ cycles for WS to reach full PEs utilization.

$$\text{Latency for WS} = 3N + S - 3 \quad (1)$$

$$\text{Throughput for WS} = \frac{2N^3}{3N + S - 3} \quad (2)$$

$$\text{Registers overhead for WS} = N(N - 1) \quad (3)$$

$$\text{TFPU for WS} = 2N - 1 \quad (4)$$

III. DiP ARCHITECTURE

In this section, we discuss DiP architecture, DiP dataflow, and DiP analytical models. Then, we compare the analytical models for DiP and WS.

A. DiP Architecture

DiP is a scalable spatial architecture consisting of $N \times N$ PEs, designed to accelerate matrix multiplication computations, as shown in Fig. 2 (a). The input matrix moves diagonally across the PEs, passing from one row of PEs to the next. The boundary PEs are diagonally connected, such that the registered inputs of the leftmost PE column are connected to the inputs of the rightmost PE column in the subsequent row. The weight matrix is loaded vertically, and psums are accumulated vertically. Figure 2 (b) shows the architecture of each PE. The proposed PE uses a 2-stage pipelined MAC unit to perform multiply and accumulate operations. It employs four enabled registers for weight, input, multiplier output, and adder output. The weight and input registers are 8-bit, while the multiplier and adder registers are 16-bit. Control signals $wshift$, pe_en , mul_en , and $adder_en$ manage the PE operations. Specifically, $wshift$ enables the weight register, while pe_en enables the input register. mul_en and $adder_en$ selectively enable their respective registers only during active computation cycles, reducing power consumption during inactive cycles. The $wshift$ signal is shared across all PEs in the systolic array, whereas pe_en , mul_en , and $adder_en$ are shared across each row.

B. DiP Dataflow

The proposed DiP architecture adopts a novel dataflow to control the movement of inputs, weights, and partial summations across the whole systolic array. DiP dataflow relies on two major upgrades compared to WS dataflow, the diagonal movement of input matrix, and the weight matrix permutation. Firstly, the input matrix moves diagonally across PE rows, as shown in Fig. 2 (a). Secondly, the proposed dataflow permutes the weights by shifting and rotating each column by its column index, as shown in Fig. 2 (c). The

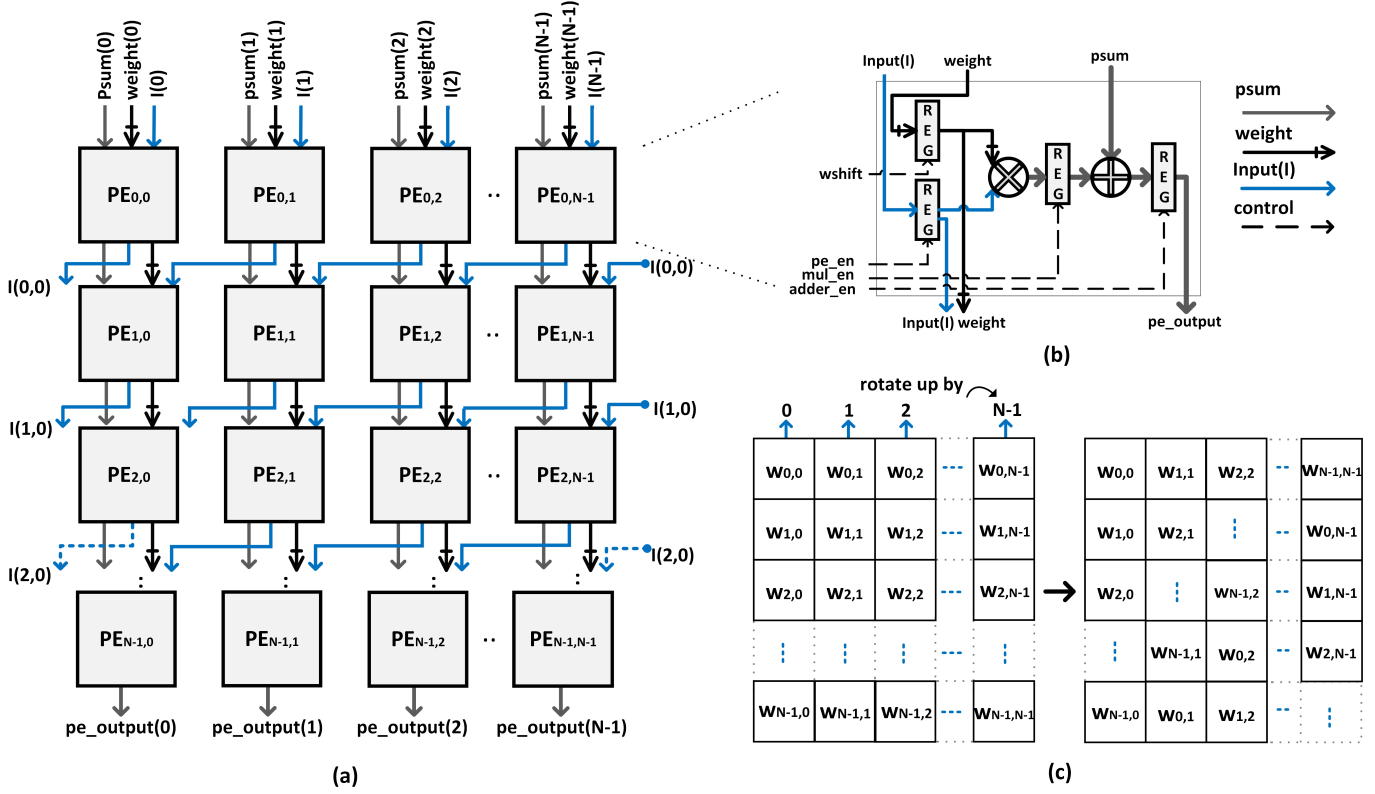


Fig. 2. (a) General $N \times N$ DiP systolic array architecture, inputs(I) move diagonally across PE rows, transitioning from one row to the next. The boundary PEs are diagonally connected, so that the registered inputs from the leftmost PE column feed into the inputs of the rightmost PE column in the subsequent row. Weights are loaded vertically, and psums are accumulated vertically along the columns as well. (b) PE block diagram, consisting of 2-stage pipelined MAC unit and four enabled registers. Control signals $wshift$, pe_en , mul_en , and $adder_en$ are used for operations control. $wshift$ is shared between all systolic array PEs, while pe_en , mul_en , and $adder_en$ are shared across each PE row. The grey buses represent the partial sum (psum) buses, while the weight buses are indicated by black crossed buses. Additionally, the input data buses are shown in blue, and control signals are represented with dashed lines. (c) General weight matrix permutation for DiP dataflow. The weight matrix is permuted by shifting and rotating each column by its column index

Pseudo code for weight matrix permutation

```

INPUT: Matrix
OUTPUT: Permuted Matrix
for i in range(cols):
  for j in range(rows):
    permuted_matrix[j][i] = matrix[(j + i) % rows][i]

```

Fig. 3. Pseudocode for weight matrix permutation, where each column undergoes an incremental row shift based on the column index, creating a unique, wrap-around pattern across rows.

weights permutation is prepared offline on software level according to the permutation pseudo code in Fig. 3. For each column, it iterates over all rows, assigning each element in the *permuted_matrix* based on its row and column index. The permutation is done at software level or at run-time in memory at almost zero cost. This permutation eliminates the input and output synchronization FIFOs required by conventional WS systolic arrays. Moreover, it increases the PE utilization and throughput, and decreases the required chip area and latency.

Figure 4 shows a complete example for 3×3 DiP systolic array. It consists of three rows: a) Row-0: PE_{00} , PE_{01} , PE_{02} , b) Row-1: PE_{10} , PE_{11} , PE_{12} , c) Row-2: PE_{20} , PE_{21} , PE_{22} . The PE array is diagonally connected, as shown in Fig. 4 (a). The leftmost PE in each PE row is connected to

the rightmost PE in the next PE row. The weight matrix is initially permuted to be prepared for weights loading. Each column is shifted and rotated by its column index, as shown in Fig. 4 (b). The weights are initially loaded, row by row, to the systolic array, as shown in Fig. 4 from *Cycle -2* to *Cycle 0*. The loading of the last weight row and the loading of first input matrix are performed in parallel at *Cycle 0*. The input data is loaded in parallel to Row-0 including inputs for PE_{00} , PE_{01} , and PE_{02} . After accomplishing the required computations by Row-0, the input data is shifted diagonally from PE_{00} to PE_{12} and from PE_{01} to PE_{10} and from PE_{02} to PE_{11} . Then after accomplishing the required computations by Row-1, the input data is shifted diagonally again from PE_{10} to PE_{22} and from PE_{11} to PE_{20} and from PE_{12} to PE_{21} . The processing starts from *Cycle 1* to *Cycle 5*, while the first output row becomes ready at *Cycle 3*, and the last output row becomes ready at *Cycle 5*. The processing goes as follows:

- **Cycle -2:** The last row of weight matrix (c, d, h) is loaded to the first PE row.
- **Cycle -1:** The last row of weights matrix (c, d, h) is shifted to the second PE row, and new weights row (b, f, g) is loaded to the first PE row.
- **Cycle 0:** The last row of the weight matrix (c, d, h) is shifted to the last PE row, the weights in the first PE

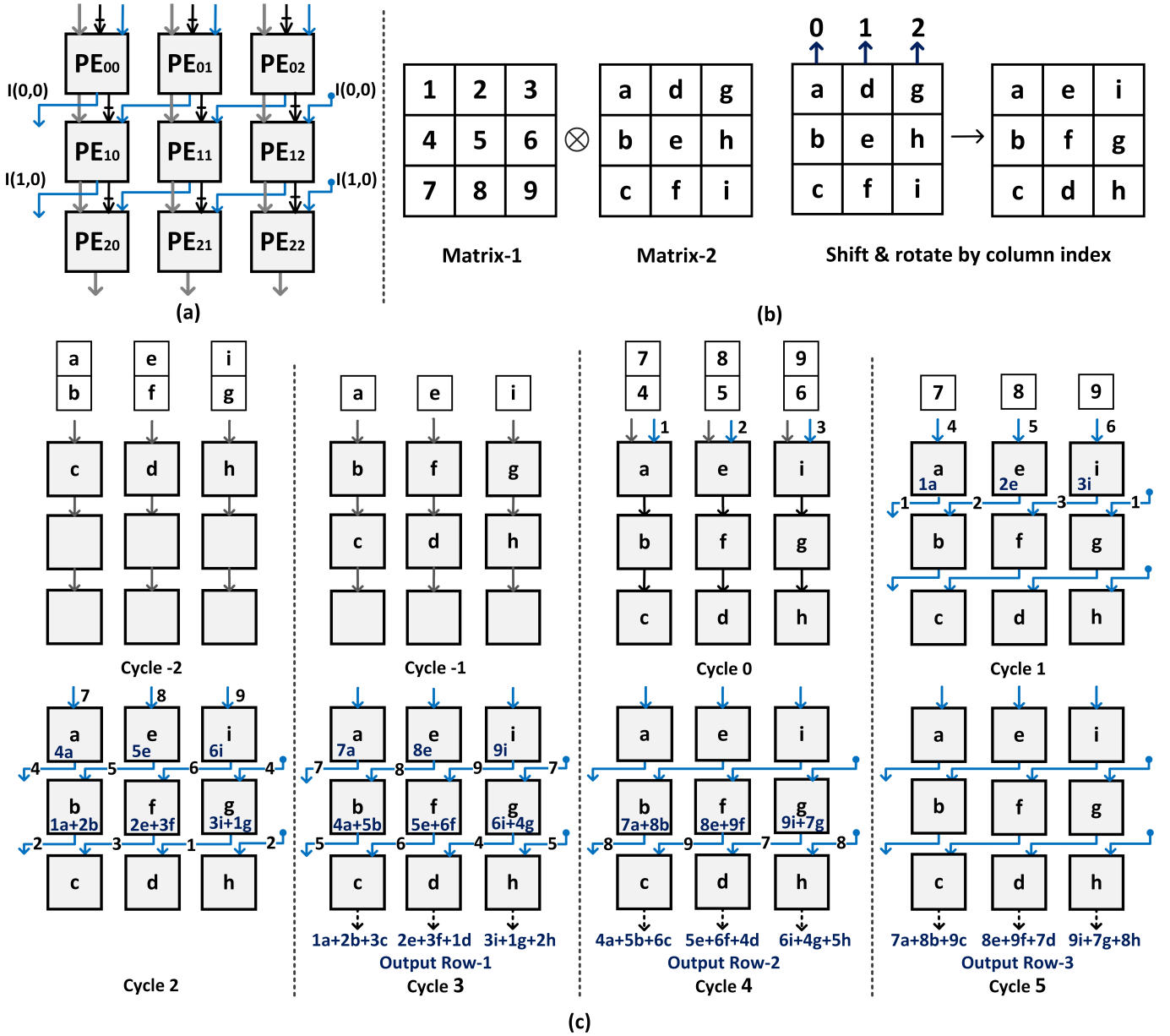


Fig. 4. Example for 3x3 DiP systolic array (a) shows the diagonal input connections for 3x3 DiP, (b) shows 3x3 DiP weight matrix permutation by shifting and rotating each column by its column index, and (c) shows the processing flow for 3x3 DiP example cycle by cycle. Cycles (-2, -1, 0) are dedicated to weight matrix loading, while Cycle 0 involves loading the last row of the weight matrix and the first row of the input matrix. Cycles from Cycle 1 to Cycle 5 are allocated for matrix multiplication processing, with final output rows becoming ready starting from Cycle 3.

row (b, f, g) are shifted to the second PE row, and new weights row (a, e, i) is loaded to the first PE row. To save one cycle, the first input matrix row ($1, 2, 3$) is loaded to the first PE row, simultaneously.

- **Cycle 1:** The first PE row shifts the partial summations ($1a, 2e, 3i$) to the second row. Using the diagonal connections, the input matrix row ($1, 2, 3$) is permuted to ($2, 3, 1$), and loaded to the second PE row at the same cycle.
- **Cycle 2:** The first PE row shifts the partial summations ($4a, 5e, 6i$) to the second row, and the input matrix row ($4, 5, 6$) is permuted to ($5, 6, 4$) and loaded to the second PE row. Similarly, The second PE row shift the partial

summations ($1a+2b, 2e+3f, 3i+1g$) to the third row, and the input matrix row ($2, 3, 1$) is permuted to ($3, 1, 2$) and loaded to the third PE row.

- **Cycle 3:** The first PE row shift the partial summations ($7a, 8e, 9i$) to the second row, and the input matrix row ($7, 8, 9$) is permuted to ($8, 9, 7$) and loaded to the second PE row. Similarly, The second PE row shift the partial summations ($4a+5b, 5e+6f, 6i+4g$) to the second row, and the input matrix row ($5, 6, 4$) is permuted to ($6, 4, 5$) and loaded to the third PE row. In addition, The third PE row shift the first output row ($1a+2b+3c, 2e+3f+1d, 3i+1g+2h$).
- **Cycle 4:** The first PE row becomes idle, unless more input

rows are loaded, and the second PE row shift the partial summations ($7a+8b$, $8e+9f$, $9i+7g$) to the third row, and the input matrix row (8 , 9 , 7) is permuted to (9 , 7 , 8) and loaded to the third PE row. In addition, the third PE row shift the second output row ($4a+5b+6c$, $5e+6f+4d$, $6i+4g+5h$).

- **Cycle 5:** The first and second PE rows are idle, and the third PE row shift the third output row ($7a+8b+9c$, $8e+9f+7d$, $9i+7g+8h$).

Meanwhile, more new inputs may loaded if the input matrix is larger, and the processing continues till the end of the workload.

C. DiP Analytical Model

The analytical models for DiP are studied for latency and throughput. Regarding DiP latency, DiP systolic array consumes $2N+S-2$ cycles for processing, where N is the number of rows/columns per DiP systolic array, and S is the number of pipelined stages per MAC unit. As a result, it takes $2N-1$ cycles for 1-stage pipelined PE, and $2N$ cycles for 2-stage pipelined PE, as shown in (5). The throughput is calculated as the number of operations (multiplications and additions) divided by the latency, as shown in (6). TFPU is calculated, as shown in (7), where it takes N cycles to reach full PEs utilization, outperforming WS by $N - 1$ cycles. For the FIFO overhead, DiP systolic array eliminates the FIFOs overhead passing the whole input row in parallel without using any input synchronization FIFOs. Correspondingly, the output is generated row by row without any need of output synchronization FIFOs.

$$\text{Latency for DiP} = 2N + S - 2 \quad (5)$$

$$\text{Throughput for DiP} = \frac{2N^3}{2N + S - 2} \quad (6)$$

$$\text{TFPU for DiP} = N \quad (7)$$

D. DiP/WSSA Analytical Comparison

The scalability of systolic arrays is important to meet the acceleration requirements. The proposed systolic array is gradually scaled up from 3×3 to 64×64 with sizes (3×3 , 4×4 , 8×8 , 16×16 , 32×32 , 64×64). An analytical comparison of DiP and WS is conducted, evaluating throughput, latency, register savings, and TFPU across different systolic array sizes. Figure 5 (a) shows the latency for DiP compared to WS, with the percentage of latency savings calculated as the difference between WS and DiP latencies, divided by WS latency. The saved percentage starts at 28% for a 3×3 systolic array and reaches 33% for a 64×64 systolic array.

In addition, The throughput for both the DiP and WS systolic arrays is compared, as shown in Fig. 5 (b). The throughput improvement is calculated as the ratio between DiP to WS throughput. The improvement ratio starts at 33.3% for a 3×3 systolic array and reaches 49.2% for a 64×64 systolic array. The proposed architecture significantly increases the PEs utilization. Thus, it outperforms the conventional WS counterparts in terms of throughput by up to 50%.

Moreover, Fig. 5 (c) shows the percentage of saved registers as another design improvement of the proposed design compared to WS systolic array. By eliminating input/output FIFOs leading to percentage of saved registers reach up to 20% for 64×64 systolic array. The saved registers is calculated as the difference between WS and DiP used registers, divided by the number of registers used by WS. The registers of WS systolic array is distributed between input synchronization FIFOs, Output synchronization FIFOs, and internal PE registers. In contrast, the proposed diagonal input systolic array relies solely on internal PE registers, eliminating the need for input/output FIFOs. The represented number of registers are normalized to 8-bit as the baseline bandwidth.

TFPU calculates the required number of cycles to reach full utilization of PEs. This metric shows the overhead when the inputs are initially loaded, particularly for large matrix-matrix multiplication. Figure. 5 (d) shows TFPU for WS and DiP systolic arrays. The proposed DiP rapidly utilizes all PEs row by row, whereas WS gradually activates PEs in a diagonal pattern, starting from the top-left and moving to the bottom-right. Consequently, DiP outperforms WS, requiring only almost half the time of WS to fully utilize the entire systolic array.

IV. EVALUATION & RESULTS

This section explores the hardware design space for the proposed DiP architecture, followed by benchmarking DiP using transformers and evaluating it against TPU-like architecture across various transformer workloads. Finally, DiP is compared with existing accelerators in the literature.

A. Hardware Design Space Exploration

A hardware design space exploration is developed for DiP and WS at different sizes. Both designs are scaled from 4×4 to 64×64 with variants (4×4 , 8×8 , 16×16 , 32×32 , 64×64). A parameterized HDL design using Verilog is developed. Then, all designs are implemented from synthesizer to GDSII using commercial 22nm technology at frequency of 1GHz. Table I shows a comparison between WS and DiP at different sizes in terms of area and power consumption. Additionally, the saved area and power consumption are presented for each design. It is depicted that the saved area percentage reach up to 8.12%. For the power consumption, the saved percentage reaches up to 19.95%.

Table II presents improvements in throughput, power consumption, area, and overall improvement (energy efficiency per area) for different WS/DiP design space. DiP outperforms WS across all metrics, with overall performance from 1.7x to 2.02x. At a size of 32×32 , DiP achieves 1.48x higher throughput than WS, 1.25x lower power consumption, and 1.09x smaller area footprint, resulting in a total improvement of 2.02x. Additionally, at size of 64×64 , throughput is improved by 1.49x, power consumption is reduced by 1.21x, and area is decreased by 1.07x compared to WS, with overall improvement 1.93x.

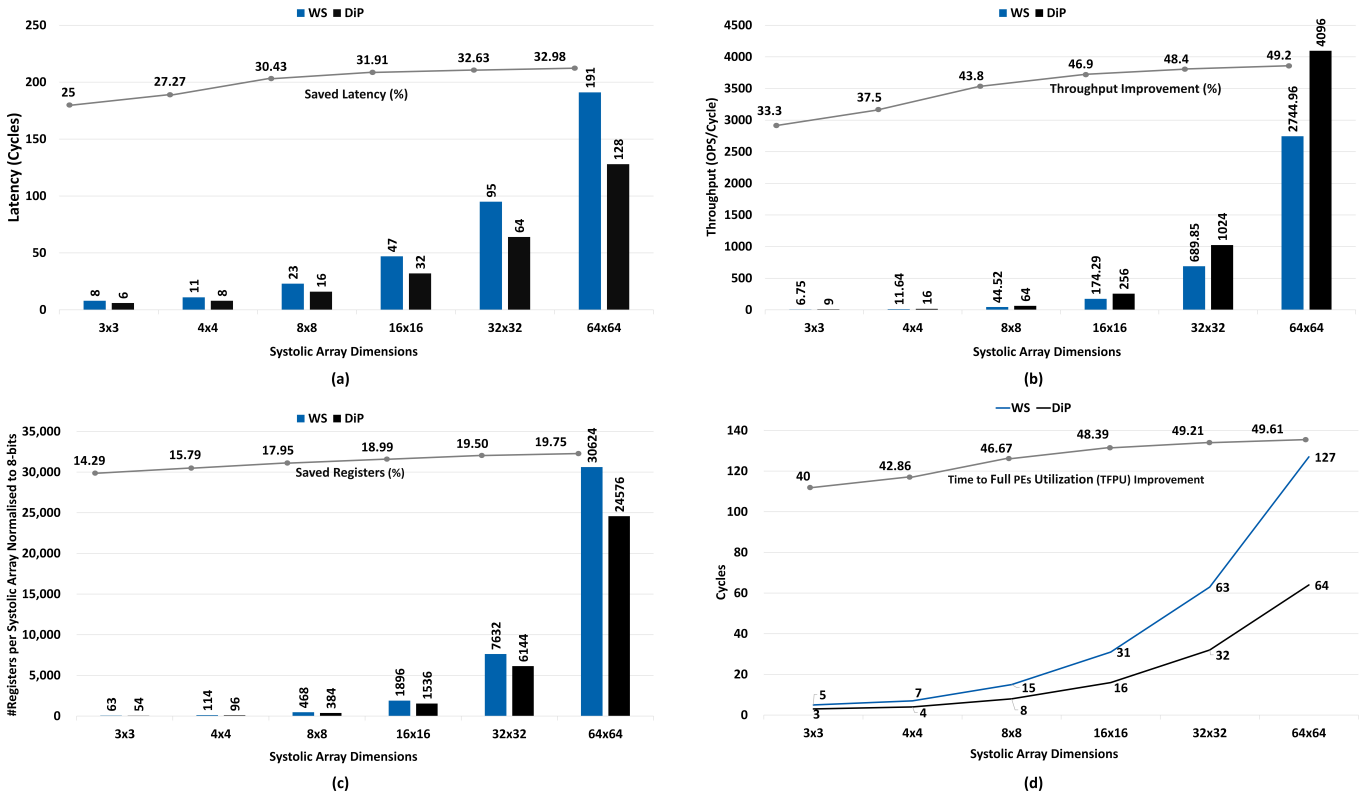


Fig. 5. (a) Latency (per single tile processing) for both WS and DiP systolic arrays. The grey curve indicates the percentage of saved latency of DiP over WS, (b) Throughput, measured in operations per cycle (OPS/Cycle), for WS and DiP, with the grey curve showing the throughput improvement percentage of DiP compared to WS, (c) The number of used registers for DiP compared to WS, normalized to 8-bit (baseline datawidth). The grey curve represents the percentage of saved registers, and (d) TFPU represented the time required to activate all PEs, with the grey curve representing the TFPU improvement percentage. WS and DiP are shown in blue and black, respectively.

TABLE I
COMPARISON OF AREA, POWER CONSUMPTION, AND SAVING PERCENTAGES FOR DIFFERENT WS/DiP SIZES USING COMMERCIAL 22NM TECHNOLOGY AT FREQUENCY OF 1GHZ

Size	Area		Saved Area (%)	Power (mW)		Saved Power Consumption (%)
	WS	DiP		WS	DiP	
4x4	5,178 (μm^2)	4,872 (μm^2)	5.91	4.168	3.582	14.06
8x8	18,703 (μm^2)	17,376 (μm^2)	7.10	16.2	13.72	15.31
16x16	71,204 (μm^2)	65,421 (μm^2)	8.12	64.28	53.63	16.57
32x32	0.275 (mm^2)	0.253 (mm^2)	7.97	264.2	211.5	19.95
64x64	1.085 (mm^2)	1.012 (mm^2)	6.73	1041	857.8	17.60

B. Transformers Benchmarking

Transformer workloads are becoming increasingly massive and heavily dependent on matrix multiplication, especially in Multi-Head Attention (MHA) and Feed-Forward Networks (FFN). MHA, a core component of transformer models proposed by Vaswani et al., enables the capture of complex dependencies in data [10]. By leveraging multiple attention heads, MHA captures diverse representational subspaces, allowing the model to understand relationships across different perspectives simultaneously.

In MHA, the input X is first projected in Queries (Q_i), Keys (K_i), and Values (V_i) per each head i using learned weight matrices, as shown in (8.1). The attention scores (S_i) for each head are computed by taking the scaled dot product of Queries (Q_i) and transposed Keys (K_i), followed by a softmax normalization, as described in (8.2). The attention scores (S_i) are multiplied with Values (V_i), producing the attention output $Attn_i$ for each head according to (8.3). The outputs from all heads are concatenated into a single matrix $Attn_{\text{concat}}$ (8.4), which is finally projected back to the model's hidden dimension (d_{model}) using a learned output projection

TABLE II
IMPROVEMENTS IN THROUGHPUT, POWER CONSUMPTION, AREA, AND OVERALL PERFORMANCE OF DiP COMPARED TO WS AT DIFFERENT SIZES

Size	Throughput Improvement (×)	Power Consumption Improvement (×)	Area Improvement (×)	Overall Improvement* (×)
4x4	1.38	1.16	1.06	1.70
8x8	1.44	1.18	1.08	1.84
16x16	1.47	1.20	1.09	1.93
32x32	1.48	1.25	1.09	2.02
64x64	1.49	1.21	1.07	1.93

*Overall improvement represents energy efficiency per area

matrix W^O , as shown in (8.5). This process enables the model to capture information from multiple representation subspaces simultaneously, enhancing the model’s ability to represent complex sequences effectively.

$$Q_i = XW_i^Q, \quad K_i = XW_i^K, \quad V_i = XW_i^V \quad (8.1)$$

$$S_i = \text{softmax}\left(\frac{Q_i K_i^T}{\sqrt{d_k}}\right) \quad (8.2)$$

$$\text{Attn}_i = S_i V_i \quad (8.3)$$

$$\text{Attn}_{\text{concat}} = \text{concat}(\text{Attn}_1, \text{Attn}_2, \dots, \text{Attn}_h) \quad (8.4)$$

$$\text{MHA} = \text{Attn}_{\text{concat}} W^O \quad (8.5)$$

Where X be the input matrix. W_i^Q , W_i^K , and W_i^V are the input projection weight matrices, and Q_i , K_i , and V_i are the resulting query, key, and value matrices per head, respectively. S_i is the score matrix, and Attn_i is the attention output per head. After concatenating all attention outputs from h heads, $\text{Attn}_{\text{concat}}$ is obtained. Finally, W^O is the output projection weight matrix, and MHA is the final multi-head attention output.

FFN in transformers consists of two linear transformations with a non-linear activation function applied between them. The process begins with the first matrix multiplication, which projects the input y into a higher-dimensional space using a weight matrix W_1 and adding bias b_1 , as shown in (9.1). Next, a non-linear activation function, such as ReLU or GELU is applied. Finally, the second matrix multiplication applies the second linear transformation to the non-linearly transformed output, mapping it back to the original dimensionality, as shown in (9.2).

$$Z = \text{Non-Linear}(yW_1 + b_1) \quad (9.1)$$

$$\text{FFN} = Z \cdot W_2 + b_2 \quad (9.2)$$

where y is the FFN input, W_1 is the first weight matrix, and b_1 is the bias. W_2 is the second FFN weight matrix and b_2 is the second bias. The output of the second transformation is the FNN result.

Table III presents the matrix multiplication dimensions for MHA and FFN operations within transformer models, highlighting the relationship between input sequence length (l), model size (d_{model}), head size (d_k), and FFN size (d_{FFN}).

TABLE III
MATRIX MULTIPLICATION DIMENSIONS FOR MHA AND FFN WORKLOADS IN TERMS OF SEQUENCE LENGTH (l), MODEL HIDDEN SIZE (d_{MODEL}), HEAD SIZE (d_k), FFN SIZE (d_{FFN}). INPUT MATRICES SIZES ARE $M \times N$ AND $N \times K$, AND OUTPUT MATRIX IS $M \times K$.

	Stage	Workload Dimensions (M, N, K)
MHA	Input projections Q_i, K_i, V_i	$l \times d_{\text{model}} \times d_k$
	Attention scores $Q_i K_i^T$	$l \times d_k \times l$
	$\text{Attn}_i = S_i V_i$	$l \times l \times d_k$
	Output projection $\text{Attn}_{\text{concat}} W^O$	$l \times d_{\text{model}} \times d_{\text{model}}$
FFN	W_1 projection	$l \times d_{\text{model}} \times d_{\text{FFN}}$
	W_2 projection	$l \times d_{\text{FFN}} \times d_{\text{model}}$

These dimensions provide insights into the computational requirements of transformer models, emphasizing how the sequence length and model size affect the matrix operations in both the attention mechanism and feed-forward network.

C. DiP Evaluation

DiP is assessed against a TPU-like (WS-based) architecture using transformer workloads. Nine widely used transformer models are chosen to span various application domains and represent a spectrum of model sizes, from small language models (SLMs) to large language models (LLMs). These models organized in three types: Encoder-Decoder, Encoder-only, and Decoder-only. Encoder-Decoder models include Vanilla Transformer [10], T5 [30], and BART [31]; Encoder-only models include BERT [35], ALBERT [36], and Transformer-XL [37]; while Decoder-only models include GPT-2 [32], GPT-3 [33], and LLaMA [34]. The models are selected with hyper-parameters to cover a diverse range of workloads. Sequence lengths are chosen from a range of 64 to 2048, as (64, 128, 256, 512, 1024, 2048). Additionally, model’s hidden size (d_{model}) varies across (512, 768, 1024, 1280, 5120), while head size (d_k) is set to either (64, 128). Moreover, FFN size (d_{FFN}) is configured with values of (2048, 3072, 4096, 5120).

DiP and TPU-like architectures, each with a size of 64x64, are used for the evaluation. This architecture size aligns well with matrix tiling, as the head size for most transformer models is either 64 or 128. Cycle-accurate simulations are performed to evaluate both DiP and TPU-like implementations in terms of actual latency for each workload and energy consumption. Matrix tiling is used to process matrix multiplication workloads on DiP and TPU-like architectures by

dividing the input matrices M_1 and M_2 into sub-matrices (tiles) of 64×64 . By studying many transformer models, the majority of MHA and FFN workload dimensions are divisible by 64. The multiplication is performed per tile as follows; For DiP and TPU-like architectures, every tile of M_2 is loaded once and remains stationary throughout the computation for the corresponding output tile. For each tile of M_2 , respective tiles from M_1 is iteratively loaded, multiplied, and saved as output partial summation (psum) tiles. After processing all tiles, the final output matrix O is constructed by accumulating the associated psum tiles.

Figure 6 compares the energy consumption and latency of DiP and TPU-like 64×64 architectures for MHA and FFN workloads across varying dimensions (M-N-K). DiP consistently outperforms TPU-like implementation for MHA and FFN workloads. Energy improvements for MHA workloads range from 1.81x for smaller workloads to 1.25x for larger ones, while FFN workloads show a similar trend with improvements from 1.8x to 1.25x. These results highlight the energy efficiency of DiP. Additionally, actual latency for MHA and FFN workloads demonstrates DiP's performance against TPU-like implementation, offering up to 1.49x improvements for smaller workloads, gradually reducing to approximately 1.03x for larger workloads. The breakdown of latency improvement

happens for larger workloads as TPU-like architecture hides the latency associated with loading more M_1 tiles per every new M_2 tile. In contrast, for small to medium-sized workloads, TPU-like architectures incur the TFPU penalty of loading M_1 tile associated with each new M_2 tile. Additionally, TPU-like architectures still face the overhead of Input/Output FIFOs, which impact power consumption, latency, and TFPU. The evaluation highlights DiP as an energy-efficient design, making it a compelling alternative to TPU-like architectures.

D. Comparison with Related Work

Table IV compares DiP architecture with Google TPU [23], Groq ThinkFast TSP [38], and Alibaba Hanguang 800 [39], highlighting DiP's performance and energy efficiency. The DiP architecture features 4,096 MACs in a 64×64 configuration, operating at 1 GHz with INT8 precision on 22nm technology. As each accelerator is implemented in different technology, the performance metrics are normalized to 22nm using DeepScaleTool [40]. The proposed DiP achieves significant energy efficiency, reaching 9.55 TOPS/W, and delivers a normalized performance per area of 8.2 TOPS. This demonstrates its capability to provide high computational throughput while minimizing energy consumption, showcasing its compact and

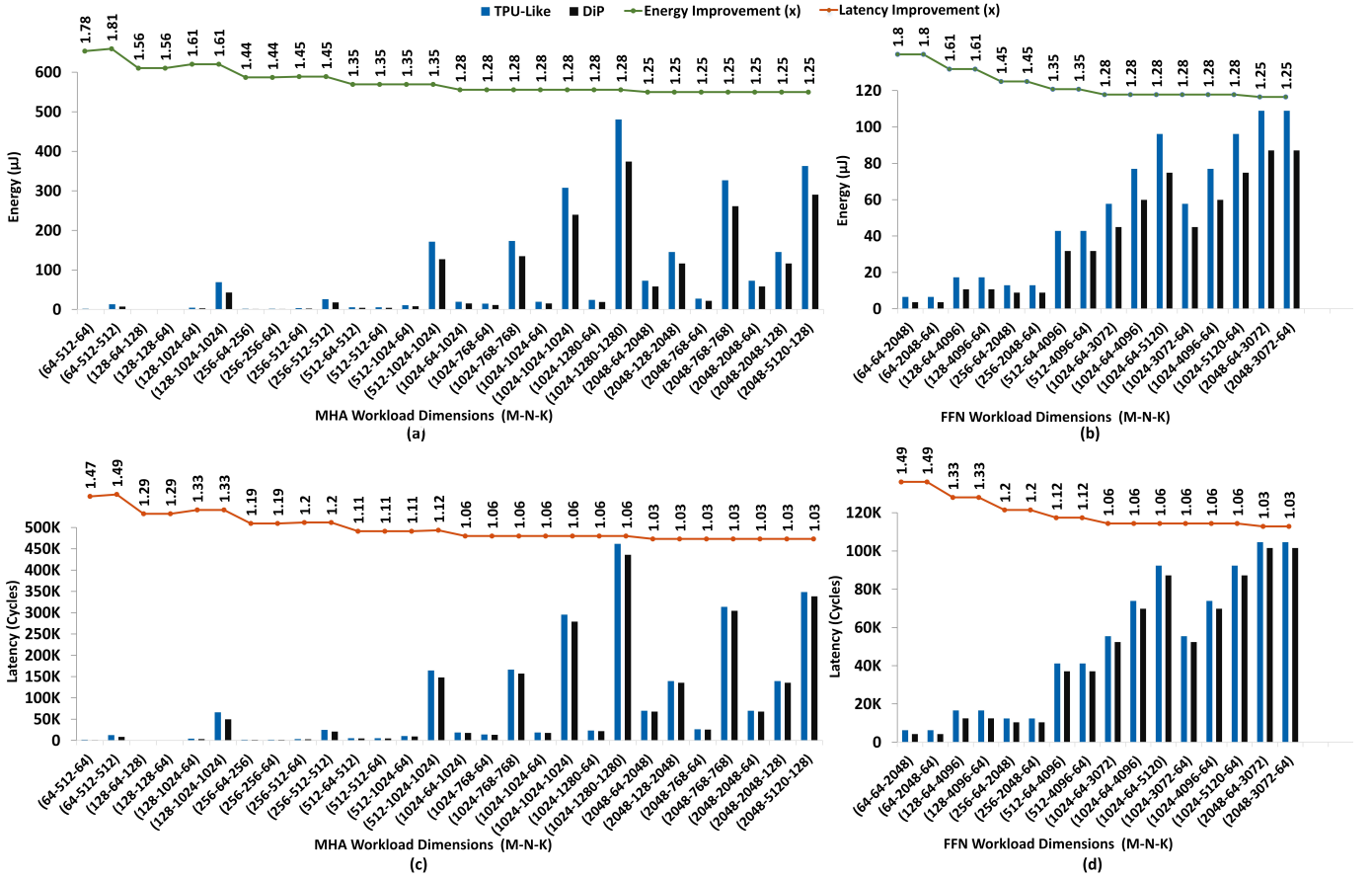


Fig. 6. Evaluation of DiP and TPU-like architecture at size 64×64 with MHA and FFN transformer's workloads. The evaluation includes actual energy consumption (a, b) and latency (c, d) across various workloads dimensions of matrix multiplication (M-N-K).

TABLE IV
COMPARISON WITH OTHER ACCELERATORS

	DiP	Google TPU [23]	Groq ThinkFast TSP [38]	Alibaba Hanguang 800 [39]
Architecture	64×64, 4,096 MACs	256×256, 65,536 MACs	Tensor Stream Processor	Tensor Cores
Max Frequency	1GHz	700MHz	900MHz	700MHz
Precision	INT8	INT8	INT8, FP16	INT8, INT16, FP24
Technology	22nm	28nm	14nm	12nm
Power (W)	0.858	40–50	300	275.9
Area (mm²)	1	200	725	709
Peak Performance (TOPS)	8.2	92	820	825
Norm. Perform. (TOPS)¹	8.2	5.75	–	–
Area Norm. Perform. (TOPS/mm²)^{2,3}	8.2	0.46	0.411	0.423
Energy Efficiency (TOPS/W)³	9.55	2.15	2.73	2.99

¹Normalized Peak Performance at systolic array size of 64×64

²Normalized Peak Performance to die area (mm²)

³Power and Area are normalized to 22nm using DeepScaleTool [40]

optimized design. These metrics make DiP particularly well-suited for energy-efficient Transformers-based applications.

V. CONCLUSION

In this paper, a diagonal-input and permuted weight-stationary (DiP) systolic array is proposed to accelerate matrix multiplication. DiP features an architecture of NxN PEs, where each PE performs Multiply-Accumulate operations. DiP adopts a novel dataflow that eliminates the input and output synchronization FIFO buffers required by the conventional WS systolic array. As a result, DiP outperforms WS across all metrics, including throughput, latency, area, and power consumption. Additionally, the analytical models for latency, throughput, FIFO overhead, and TFPU are developed for DiP and WS architectures. The proposed DiP architecture outperforms the WS counterparts in terms of throughput by up to 50%, and TFPU by up to 50%. Moreover, hardware design space exploration is presented for both DiP and WS architectures using commercial 22nm technology, demonstrating power consumption savings of up to 19.95%, area savings of up to 8.12% at 1 GHz, and energy efficiency per area improvement of up to 2.02x. Furthermore, DiP is evaluated using various transformer workloads from widely-used models such as GPT-2, GPT-3, BERT, BART, and LLaMA. DiP outperforms TPU-like architecture, achieving energy improvements ranging from 1.25x to 1.81x and latency improvements ranging from 1.03x to 1.49x across various transformer’s MHA and FFN workloads. A comparison between relevant accelerators and DiP is discussed, achieving performance of 8.2 TOPS and energy efficiency of 9.55 TOPS/W, which is promising for energy-efficient transformer-based applications. This paper serves as the foundation for DiP architecture and dataflow. Future extensions aim to scale the architecture and explore sparsity in transformers, which will further enhance energy efficiency and acceleration rates.

REFERENCES

- [1] B. Mondal, "Artificial Intelligence: State of the Art," *Recent Trends Adv. Artif. Intell. Internet Things*, vol. 172, pp. 389-425, 2020.
- [2] G. G. Chowdhury, "Natural language processing," *Annu. Rev. Inf. Sci. Technol.*, vol. 37, no. 1, pp. 51-89, 2003.
- [3] D. Khurana *et al.*, "Natural language processing: State of the art, current trends and challenges," *Multimedia Tools Appl.*, vol. 82, pp. 3713-3744, 2023.
- [4] A. Gillioz *et al.*, "Overview of the Transformer-based Models for NLP Tasks," *Proc. 15th Conf. Comput. Sci. Inf. Syst. (FedCSIS)*, pp. 179-183, 2020.
- [5] H. Zhang *et al.*, "A Survey of Controllable Text Generation Using Transformer-based Pre-trained Language Models," *ACM Comput. Surv.*, vol. 56, no. 64, 37 pages, Mar. 2024.
- [6] Y. Wang *et al.*, "Transformer in Action: A Comparative Study of Transformer-Based Acoustic Models for Large Scale Speech Recognition Applications," *Proc. IEEE Int. Conf. Acoust., Speech Signal Process. (ICASSP)*, pp. 6778-6782, 2021.
- [7] P. Xu, X. Zhu, and D. A. Clifton, "Multimodal Learning With Transformers: A Survey," *IEEE Trans. Pattern Anal. Mach. Intell.*, vol. 45, no. 10, pp. 12113-12132, Oct. 2023.
- [8] K. Han *et al.*, "A Survey on Vision Transformer," *IEEE Trans. Pattern Anal. Mach. Intell.*, vol. 45, no. 1, pp. 87-110, Jan. 2023.
- [9] T. Lin *et al.*, "A survey of transformers," *AI Open*, vol. 3, pp. 111-132, 2022.
- [10] A. Vaswani *et al.*, "Attention is all you need," *Proc. Adv. Neural Inf. Process. Syst.*, pp. 6000-6010, 2017.
- [11] J. Hoffmann *et al.*, "Training compute-optimal large language models," *Proc. 36th Int. Conf. Neural Inf. Process. Syst.*, 2024.
- [12] L. Floridi and M. Chiriatti, "GPT-3: Its nature, scope, limits and consequences," *Minds Mach.*, vol. 30, pp. 681-694, 2020.
- [13] H.-T. Kung, "Why systolic architectures?," *IEEE Comput.*, vol. 15, no. 1, pp. 37-46, Jan. 1982.
- [14] Y. H. Hu and S. Kung, "Systolic arrays," *Handbook Signal Process. Syst.*, pp. 939-977, 2018.
- [15] Z. Yang *et al.*, "Systolic array based accelerator and algorithm mapping for deep learning algorithms," *Proc. Netw. Parallel Comput.*, pp. 153-158, 2018.
- [16] M. Soltanyeh *et al.*, "An Accelerator for Sparse Convolutional Neural Networks Leveraging Systolic General Matrix-Matrix Multiplication," *ACM Trans. Archit. Code Optim.*, vol. 19, no. 3, Article 42, 2022.
- [17] B. Wang *et al.*, "A novel systolic array processor with dynamic dataflows," *Integration*, vol. 85, pp. 42-47, 2022.
- [18] H. Waris *et al.*, "AxSA: On the design of high-performance and power-efficient approximate systolic arrays for matrix multiplication," *J. Signal Process. Syst.*, vol. 93, no. 6, pp. 605-615, Jun. 2021.
- [19] G. Shomron *et al.*, "SMT-SA: Simultaneous multithreading in systolic arrays," *IEEE Comput. Archit. Lett.*, vol. 18, no. 2, pp. 99-102, Jul. 2019.

- [20] M. A. Hanif *et al.*, "MPNA: A massively-parallel neural array accelerator with dataflow optimization for convolutional neural networks," *arXiv:1810.12910*, 2018.
- [21] C. Peltekis *et al.*, "ArrayFlex: A Systolic Array Architecture with Configurable Transparent Pipelining," *Proc. Design, Autom. Test Eur. Conf. Exhib. (DATE)*, pp. 1-6, 2023.
- [22] J. Dean, D. Patterson, and C. Young, "A New Golden Age in Computer Architecture: Empowering the Machine-Learning Revolution," *IEEE Micro*, vol. 38, no. 2, pp. 21-29, 2018.
- [23] N. P. Jouppi *et al.*, "In-datacenter performance analysis of a tensor processing unit," *Proc. 44th Annu. Int. Symp. Comput. Archit.*, pp. 1-12, Jun. 2017.
- [24] N. P. Jouppi *et al.*, "A Domain-Specific Supercomputer for Training Deep Neural Networks," *Commun. ACM*, vol. 61, no. 10, pp. 67-79, 2017.
- [25] N. P. Jouppi *et al.*, "Ten Lessons From Three Generations Shaped Google's TPUv4i," *IEEE Micro*, vol. 41, no. 2, pp. 57-66, 2021.
- [26] B. Asgari *et al.*, "Meissa: Multiplying matrices efficiently in a scalable systolic architecture," *Proc. 2020 IEEE 38th Int. Conf. Comput. Design (ICCD)*, pp. 130-137, 2020.
- [27] Y. Xu *et al.*, "A Survey of Design and Optimization for Systolic Array-Based DNN Accelerators," *ACM Comput. Surv.*, vol. 56, no. 1, pp. 1-37, 2023.
- [28] E. Yago *et al.*, "Impact of the Array Shape and Memory Bandwidth on the Execution Time of CNN Systolic Arrays," *Proc. 23rd Euromicro Conf. Digit. Syst. Design (DSD)*, pp. 510-517, 2020.
- [29] Y.-H. Chen, J. Emer, and V. Sze, "Eyeriss: a spatial architecture for energy-efficient dataflow for convolutional neural networks," *Proc. 43rd Int. Symp. Comput. Archit. (ISCA)*, pp. 367-379, 2016.
- [30] C. Raffel *et al.*, "Exploring the Limits of Transfer Learning with a Unified Text-to-Text Transformer," *J. Mach. Learn. Res.*, vol. 21, no. 140, pp. 1-67, 2020.
- [31] M. Lewis *et al.*, "BART: Denoising Sequence-to-Sequence Pre-training for Natural Language Generation, Translation, and Comprehension," *arXiv preprint arXiv:1910.13461*, 2019.
- [32] A. Radford *et al.*, "Language Models are Unsupervised Multitask Learners," OpenAI, 2019. [Online].
- [33] T. B. Brown *et al.*, "Language Models are Few-Shot Learners," *arXiv preprint arXiv:2005.14165*, 2020.
- [34] H. Touvron *et al.*, "LLaMA: Open and Efficient Foundation Language Models," *arXiv preprint arXiv:2302.13971*, 2023.
- [35] J. Devlin, M.-W. Chang, K. Lee, and K. Toutanova, "BERT: Pre-training of Deep Bidirectional Transformers for Language Understanding," *arXiv preprint arXiv:1810.04805*, 2019.
- [36] Z. Lan *et al.*, "ALBERT: A Lite BERT for Self-supervised Learning of Language Representations," *arXiv preprint arXiv:1909.11942*, 2019.
- [37] Z. Dai *et al.*, "Transformer-XL: Attentive Language Models Beyond a Fixed-Length Context," *arXiv preprint arXiv:1901.02860*, 2019.
- [38] D. Abts *et al.*, "Think fast: A tensor streaming processor (TSP) for accelerating deep learning workloads," *Proc. ACM/IEEE 47th Annu. Int. Symp. Comput. Archit.*, pp. 145-158, 2020.
- [39] Y. Jiao *et al.*, "A 12nm programmable convolution-efficient neural-processing-unit chip achieving 825TOPS," *Proc. IEEE Int. Solid-State Circuits Conf.*, pp. 136-140, 2020.
- [40] S. Sarangi and B. Baas, "DeepScaleTool: A tool for the accurate estimation of technology scaling in the deep-submicron era," *Proc. IEEE Int. Symp. Circuits Syst.*, pp. 1-5, 2021.



Ahmed J. Abdelmaksoud (Member, IEEE) is currently pursuing his PhD with the Centre for Electronics Frontiers (CEF) at the University of Edinburgh, UK. He received his BSc and MSc in Electronics Engineering from Cairo University, Egypt in 2018 and 2022, respectively. Since 2018, he has been actively involved in Digital ASIC design projects across both research and industry. His professional experience includes working as a Research Associate at the System-on-Chip Center, Khalifa University, UAE; an ASIC Physical Design Engineer at Si-

vision, Egypt; and a Research Assistant at the Opto-Nano Electronics Lab, Egypt. In addition, his current research interests primarily focus on developing spatial and specialized architectures for efficient AI hardware acceleration.



Shady Agwa (Member, IEEE) is a Research Fellow at the Centre for Electronics Frontiers CEF, The University of Edinburgh (UK). He received his BSc and MSc degree from Assiut University (Egypt), both in Electrical Engineering. He got his PhD in Electronics Engineering from The American University in Cairo (Egypt) in 2018. Following his PhD, he joined the Computer Systems Laboratory at Cornell University (USA) as a Postdoctoral Associate for two years. In 2021, Shady joined the Centre for Electronics Frontiers at the University of Southampton (UK) as a Senior Research Fellow and then as a Research Fellow at the University of Edinburgh (UK). His research interests span across VLSI and Computer Architecture for AI using conventional and emerging technologies. His work focuses on ASIC-Driven AI Architectures with extensive expertise in In-Memory Computing, Stochastic Computing, Systolic Arrays, Beyond Von Neumann Architectures, Memories and Energy-Efficient Digital ASIC Design.



Themis Prodromakis (Senior Member, IEEE) received the bachelor's degree in electrical and electronic engineering from the University of Lincoln, U.K., the M.Sc. degree in microelectronics and telecommunications from the University of Liverpool, U.K., and the Ph.D. degree in electrical and electronic engineering from Imperial College London, U.K. He then held a Corrigan Fellowship in nanoscale technology and science with the Centre for Bio-Inspired Technology, Imperial College London, and a Lindemann Trust Visiting Fellowship

with the Department of Electrical Engineering and Computer Sciences, University of California at Berkeley, USA. He was a Professor of nanotechnology at the University of Southampton, U.K. He holds the Regius Chair of Engineering at the University of Edinburgh and is Director of the Centre for Electronics Frontiers. He is currently a Royal Academy of Engineering Chair in emerging technologies and a Royal Society Industry Fellowship. His background is in electron devices and nanofabrication techniques. His current research interests include memristive technologies for advanced computing architectures and biomedical applications. He is a fellow of the Royal Society of Chemistry, the British Computer Society, the IET, and the Institute of Physics.